ENVIRONMENTAL RESEARCH
LETTERS

LETTER • OPEN ACCESS

Decadal variations of Pacific Walker circulation tied to tropical Atlantic–Pacific trans-basin SST gradients

ENVIRONMENTAL RESEARCH
LETTERS

LETTER

Decadal variations of Pacific Walker circulation tied to tropical Atlantic–Pacific trans-basin SST gradients

Shuai-Lei Yao[1,*], **Jing-Jia Luo**[2], **Pao-Shin Chu**[3] **and Fei Zheng**[4,5]

[1] State Key Laboratory of Numerical Modeling for Atmospheric Sciences and Geophysical Fluid Dynamics, Institute of Atmospheric Physics, Chinese Academy of Sciences, Beijing 100029, People's Republic of China
[2] Institute for Climate and Application Research (ICAR)/CIC-FEMD, Nanjing University of Information Science & Technology, Nanjing 210044, People's Republic of China
[3] Department of Atmospheric Sciences, School of Ocean and Earth Science and Technology, University of Hawai'i at Mānoa, Honolulu, HI 96822, United States of America
[4] School of Atmospheric Sciences, Key Laboratory of Tropical Atmosphere-Ocean System, Ministry of Education, Sun Yat-sen University, Zhuhai, People's Republic of China
[5] Southern Marine Science and Engineering Guangdong Laboratory, Zhuhai 519082, People's Republic of China
[*] Author to whom any correspondence should be addressed.

E-mail: yaoshl08@hotmail.com

Keywords: Pacific Walker circulation, decadal strengthening, robust westward shift, inter-basin warming contrast

Supplementary material for this article is available online

OPEN ACCESS

RECEIVED
23 January 2023

REVISED
9 April 2023

ACCEPTED FOR PUBLICATION
28 April 2023

PUBLISHED
16 May 2023

Abstract

During the modern satellite-monitoring era since ∼1979, the observed Pacific Walker circulation (PWC) presented a pronounced strengthening and robust westward-shifting, defying the model-projected weakening response to anthropogenic warming. The exact cause for the PWC decadal intensification and the corresponding observation-model disagreement remains indecisive. Using two targeted experiments wherein sea surface temperature (SST) anomalies in the tropical eastern Pacific and North Atlantic are separately restored to follow the observed history, we reveal that the North Atlantic-only SST warming and the tropical eastern Pacific-only SST cooling contribute partly to the PWC decadal adjustment. The North Atlantic SST warming triggers a significant westward displacement of PWC, while the tropical eastern Pacific SST cooling drives mainly the associated shifts of the large-scale atmospheric surface pressure centers. Further, we identify that the tropical Atlantic–eastern Pacific trans-basin SST gradients have dominated the PWC decadal variations over the past century. Our results highlight that a reliable representation of the simulated inter-basin warming contrast between the tropical Atlantic and the tropical eastern Pacific SSTs may be influential in correcting future projections of the PWC strength.

1. Introduction

The Pacific Walker circulation (PWC) is an integral, key part of the tropical climate system. On the inter-annual timescales, the east-west zonally-oriented atmospheric overturning circulation is inextricably linked to the El Niño-Southern Oscillation (Bjerknes 1969). For an El Niño case, it features anomalous ascending over the central equatorial Pacific and anomalous subsidence over the Maritime Continent and the Amazon basin, accompanied by surface westerlies along the equator and easterlies in the upper troposphere (Chu and Murakami 2022). The opposite holds for a La Niña event. Indeed, for the continuous satellite-monitoring period available since ∼1979, the observed PWC has experienced a conspicuous intensification (L'Heureux *et al* 2013). Associated with the decadal-scale reorganization of PWC is a great strengthening of tropical Pacific trade winds (De Boisséson *et al* 2014), driving unusually rapid sea-level rise over the tropical western Pacific (Merrifield 2011) and enhanced heat transport into the upper Indian Ocean from the tropical Pacific (Lee *et al* 2015), creating favorable conditions for the 2013 super-typhoon Haiyan sweeping the Philippines (Lin *et al* 2014) and devastating

decade-long droughts across western North America (Delworth *et al* 2015). It also causes the increased Amazon flooding extremes (Barichivich *et al* 2018) and a shift toward drying eastern Africa (Williams and Funk 2011) and contributes to the early 2000s global warming slowdown (England *et al* 2014, Watanabe *et al* 2014, Fyfe *et al* 2016, Yao *et al* 2017). Given these climatic consequences worldwide, understanding the underlying mechanism driving the PWC decadal adjustment is instrumental for future climate change projections.

Hitherto, four leading hypotheses have emerged regarding the PWC decadal changes. The first suggests a long-term weakening of the PWC due to a muted hydrological response to greenhouse warming (Held and Soden 2006, Vecchi *et al* 2006), opposing the observed PWC decadal strengthening in recent decades. The second considers an ocean dynamical thermostat-type effect (Clement *et al* 1996, Luo *et al* 2017, Seager *et al* 2019). Specifically, sea surface temperature (SST) over the equatorial western Pacific warms faster than the eastern Pacific cold tongue due to the *in-situ* cold water upwelling. The accelerated west-east SST gradient induces a transient PWC strengthening that may last about 20–30 years under abrupt CO_2 increases (Heede *et al* 2020), despite a large discrepancy between the abruptly-perturbed climate system and the real world. The third ascribes the PWC decadal strengthening to internal decadal climate modes (Chung *et al* 2019), such as the cold-phase Inter-decadal Pacific Oscillation (IPO) (England *et al* 2014) or the warm-phase Atlantic multi-decadal variability (AMV) (Kucharski *et al* 2016, Meehl *et al* 2021), although these statistical results have yet to be rigorously validated. The last primarily attributes the PWC decadal intensification to inter-basin SST variabilities triggered by basin-wide SST warming over the Atlantic (Kucharski *et al* 2011, McGregor *et al* 2014, Li *et al* 2016) or the Indian Ocean (Luo *et al* 2012). However, a broader view is required to reconcile the respective importance of decadal climate modes and inter-basin SST variabilities in pacing the timing and magnitude of observed PWC.

By combining multiple reanalysis datasets with a hierarchy of coupled climate model simulations, we carry out a physically consistent, integrated study on the PWC decadal change, enabling us to resolve the intense debate on the extent to which the internal decadal climate modes or trans-basin SST variabilities act as a main driver of the PWC decadal variation. These results, supported by observations and pacemaker simulations (Meehl *et al* 2021), indicate that the PWC decadal variation relies heavily on the tropical Atlantic-eastern Pacific trans-basin SST gradients rather than on SST changes solely in one basin.

2. Datasets, analysis methods, and model experiments

2.1. Reanalysis datasets

The PWC decadal changes are explored using four reanalysis datasets, including the NOAA 20th-century reanalysis product version 3 throughout 1900–2013 (Slivinski *et al* 2019), ERA-interim, ERA5 (Dee *et al* 2011), and JRA-55 (Kobayashi *et al* 2015) covering 1979–2013. The monthly-mean precipitation from GPCP version 2.3 (Adler *et al* 2003) provides the physical coherence with the PWC decadal changes to sea level pressure (SLP) and 850 hPa winds. We utilize seven SST datasets spanning from 1900 to 2013, including ERSST v3b, v4, and v5 (Huang *et al* 2015, 2017), COBE-SST and COBE-SST 2 (Hirahara *et al* 2014), the Hadley Center Sea Ice and SST (Titchner and Rayner 2014), and Hurrell SST (Hurrell *et al* 2008). Owing to observational uncertainties among different SST datasets, we use the multiple SST ensemble mean to estimate the Atlantic–Pacific trans-basin warming contrast.

2.2. PWC strength

We measure the PWC strength by utilizing the following three indices. The first is defined as area-averaged 850 hPa zonal winds across the western-central equatorial Pacific (6° S–6° N, 150° E–210° E) (Luo *et al* 2012). Negative values indicate easterly anomalies, suggestive of an accelerated PWC. The second is derived from the area-averaged zonal SLP difference between the eastern equatorial Pacific (5° S–5° N, 160° W–80° W) and western Pacific/eastern Indian Ocean (5° S–5° N, 80° E–160° E) (Vecchi *et al* 2006). Positive values denote increased trans-basin SLP gradients, representing an intensified PWC. The third employs the zonal mass stream function to display an integral three-dimensional structure of PWC (Yu and Zwiers 2010) as follows:

$$\psi = \frac{a\Delta\varphi}{g}\int_0^p u_{\mathrm{d}}\mathrm{d}p$$

where ψ indicates the zonal mass stream function, a is the radius of the Earth, g is the gravitational acceleration, $\Delta\varphi = 2\pi \cdot \frac{10}{360}$ (the radian between 5° S–5° N), u_{d} is the divergent component of zonal wind, and p is the pressure. The zonal mass stream function is estimated by integrating meridional-mean divergent wind from the top level downward. Positive values depict a clockwise overturning circulation in the zonal-vertical section.

2.3. IPO and AMV indices

The SST-based IPO and AMV indices are estimated from the internally-generated components of observed IPO-SST and AMV-SST anomalies

(figure S1). We first apply the signal-to-noise maximizing empirical orthogonal function (EOF) analysis to global annual-mean SST from the multi-model ensemble mean of CMIP5 historical simulations (1870–2005) and Representative Concentration Pathway 8.5 (RCP8.5; 2006–2013) (Ting *et al* 2009, Ruprich-Robert *et al* 2017, Yao *et al* 2021, 2022), and extract the radiatively-forced response. After removing the externally-forced component from the observed SST (ERSST v3b), the IPO and AMV indices are derived from the first principal component of an EOF decomposition to the observed annual-mean residual SST over the Pacific-wide domain (40° S–60° N, from Indonesia to the American Coast) and North Atlantic (0°–60° N, from the American coast to Africa/Europe), respectively. Finally, we construct the IPO and AMV spatial patterns by regressing the observed residual SST at each grid point against the IPO and AMV indices, respectively. Note that the IPO and AMV time series have been low-pass filtered by applying a zero-phasing Butterworth filter before the regression.

To untangle the potential linkage of PWC decadal changes to the Pacific and Atlantic decadal climate modes, we estimate the PWC strength congruent to IPO and AMV for 1979–2013, over which the IPO shifts its phase from positive to negative, and the AMV translates its phase from negative to positive (figure S1). We first regress the PWC intensity (including 850 hPa zonal winds and SLP) at each grid point against the IPO and AMV indices for 1900–2013, respectively. Subsequently, the corresponding regression coefficients for the IPO and AMV are separately multiplied by the observed IPO and AMV trends of 1979–2013. This method allows us to directly quantifies how much of the observed PWC decadal changes are due to the IPO or AMV.

2.4. Pacemaker experiments

To enhance our understanding of trans-basin SST variability generated by each ocean basin in modulating the PWC decadal changes, we analyze three pacemaker experiments with CESM1 following an identical pacemaker experimental protocol (Kosaka and Xie 2013, Deser *et al* 2017, Meehl *et al* 2021). In these three pacemaker simulations (table S1), SST anomalies over the tropical Indian Ocean-Western Pacific (IOWP: 15° S–15° N, from the eastern African coast to 180° E with 5° sponge zones in northern, southern, and eastern boundaries), the eastern tropical Pacific (TEP: 15° S–15° N, 180° to the American coast with 5° sponge zones in northern, southern, and western boundaries) and North Atlantic (ATL: 0°–60° N, from the American coast to Africa/Europe with 5° buffer zones in southern and northern boundaries) are separately restored to observations (figure S2). Outside the targeted regions, the ocean-atmosphere systems are fully coupled. Each simulation is also forced with time-varying historical radiative forcing for 1920–2005 and RCP8.5 for 2006–2013 and comprises ten ensemble members initialized with slightly different initial atmospheric conditions. The three pacemaker runs are compared with the 35-member historical simulations to determine to what degree the trans-basin SST variability drives the PWC decadal variations. All the trend results shown here are computed using Sen's slope method, with a 95% statistical significance using the Mann–Kendall test (Chu *et al* 2010).

3. Results

3.1. The relative importance of IPO and AMV

Examining the running-window 35 year trends of observed PWC intensity, derived from 850 hPa zonal winds averaged over the western-central equatorial Pacific and the zonal SLP difference between the equatorial eastern Pacific and western Pacific/eastern Indian Ocean, we track the timing and magnitude of observed PWC decadal evolutions. For ease of comparison, the first year of 35 year trends of two indices is shown in figure 1(a). Decadal changes in the 850 hPa winds and inter-basin SLP gradients are highly correlated over the past century ($r = -0.92$, significant at $P < 0.05$ in figure 1(a)). The observed PWC strength exhibits considerable multi-decadal variations, with a noticeable decline from the 1900s until the 1950s and a rising tendency from the 1960s onwards. However, the observed PWC strength is more susceptible to a large uncertainty before 1920, mainly due to insufficient data coverage (Slivinski *et al* 2019). During 1979–2013, the observed PWC underwent a robust intensification (Ma and Zhou 2016, Li *et al* 2021), opposing the externally-forced weakening response to greenhouse warming from single-model and multi-model ensemble historical simulations (figure S3). The marked observation-model discrepancy implies that external forcing is not the major contributor to a significant strengthening of observed PWC for 1979–2013.

We further investigate the role of internal variability by putting the IPO and AMV into the context of observed PWC historical evolutions. Specifically, first regressing the observed 850 hPa zonal winds and SLP at each grid onto the observed IPO and AMV indices for 1900–2013 and then multiplying the resulting regression coefficients by the running-window 35 year trends in the observed IPO and AMV indices, we quantify the respective fraction of observed PWC decadal trends that are linearly congruent with the IPO and AMV. For 1900–2013, the probability density functions of the observed and AMV-induced 35 year PWC trends are roughly analogous but much broader than the IPO-induced trends (figures 1(b) and (c)), mainly due to a larger spread for the 35 year AMV trends caused by less frequent phase shifts of AMV index (figures S1(c)–(e)). Over 1979–2013, the 35 year IPO trend (−3.40) is extremely rare (figure

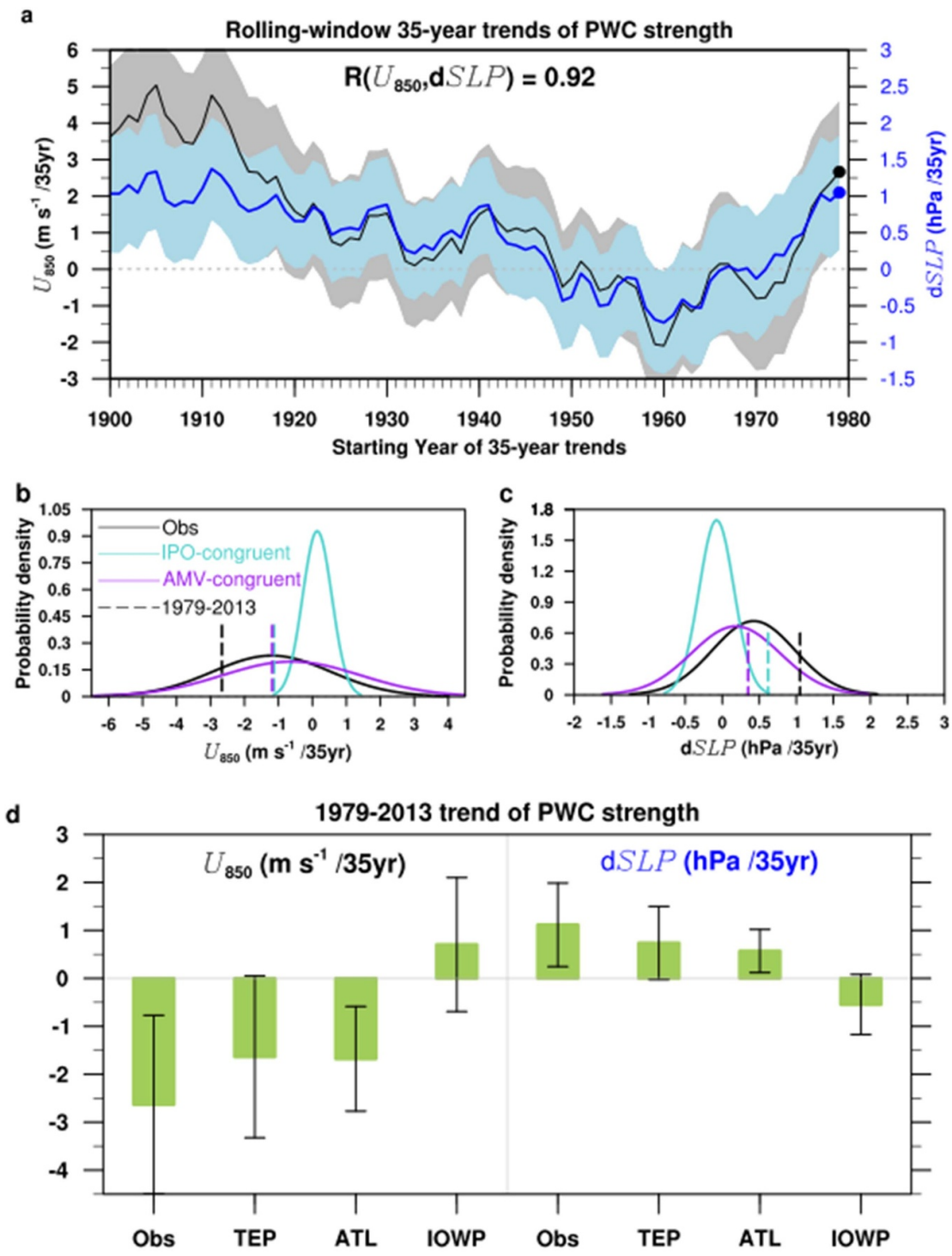

Figure 1. (a) Moving-window 35 year trends of the observed Pacific Walker circulation (PWC) strength shifting from 1900–1934–1979–2013 (dots), measured by the 850 hPa zonal winds averaged over the western-central equatorial Pacific (6° S–6° N, 150° E–210° E) (solid black line) and the area-averaged zonal SLP difference along the equator between the eastern Pacific (5° S–5° N, 160° W–80° W) and eastern Indian Ocean/western Pacific (5° S–5° N, 80° E–160° E) (solid blue line). The colored shading denotes the 95% confidence interval. Note that the 850 hPa zonal wind trends are multiplied by −1 to facilitate comparison with the trans-basin SLP gradients. (b) Smoothed normalized distribution of 35 year trends of 850 hPa zonal winds from the NOAA 20th reanalysis version 3 (black curve) and congruent to the observed IPO (IPO-congruent; cyan) and AMV (AMV-congruent; purple) trends, respectively. Dashed lines indicate 1979–2013 trends. As the AMV-induced 1979–2013 wind trend (−1.19 ms^{-1}/35 yr in purple dashed line) and the IPO-induced wind trend (−1.13 ms^{-1}/35 yr in cyan dashed line) are almost equal, the two dashed lines slightly overlap. (c) same as (b) but for running-window 35 year trends of the area-averaged SLP difference. (d) Observed and simulated 1979–2013 trends of PWC strength from an ensemble mean of four different reanalysis datasets (Obs), a ten-member ensemble of tropical eastern Pacific pacemaker simulations (TEP), a ten-member ensemble of North Atlantic Ocean pacemaker simulations (ATL), and a ten-member ensemble of tropical IOWP pacemaker simulations (IOWP). The error bars indicate the 95% confidence intervals.

S1(e)), leading to the IPO-induced PWC trends falling into the left tail of the probability density function, while the 35 year AMV trend (1.28) is relatively moderate, making the AMV-induced PWC trends falling within the middle of the probability density function.

Because this period matches well with a positive-to-negative phase shift of IPO and a negative-to-positive phase transition of AMV, we also isolate the respective contributions of the IPO and AMV phase transitions to PWC decadal accelerations by analyzing the ten-year idealized IPO and AMV pacemaker experiments, wherein SST anomalies over the Pacific and North Atlantic are separately restored to the internally-driven components of observed IPO-SST and AMV-SST anomalies while holding all radiative forcing fixed at pre-industrial level (see more details in text S1 of supplementary information) (Boer *et al* 2016, Ruprich-Robert *et al* 2017, Meehl *et al* 2021, Yao *et al* 2021, 2022). The simulated warm-to-cold phase shift of IPO or cold-to-warm phase transition of AMV partly accounts for the observed PWC decadal strengthening of 1979–2013 (figure S4), with the former being larger than the latter, although potential model biases may slacken the simulated PWC responses to the IPO-SST and AMV-SST forcing (Boer *et al* 2016, Yao *et al* 2021, 2022). The results diagnosed by statistical analysis and idealized pacemaker simulations provide evidence that the IPO or AMV alone cannot fully trigger the observed PWC decadal strengthening over 1979–2013.

3.2. The role of trans-basin SST variabilities

For 1979–2013, the observed trade winds over the western-central equatorial Pacific are intensified by -2.63 ms^{-1}/35 yr, and the trans-basin SLP gradients are enhanced by 1.12 hPa/35 yr based on the ensemble mean of four reanalysis datasets (figure 1(c)). The observed PWC intensity is well reproduced by a 44-model ensemble of global SST anomaly-driven atmosphere-only experiments from the latest sixth Atmospheric Model Inter-comparison Project (figures S4 and S5). To more accurately single out the respective contributions of trans-basin SST variabilities triggered by each ocean basin to the PWC decadal strengthening, we systematically examine three pacemaker experiments, wherein SSTs over the tropical eastern Pacific, North Atlantic, and tropical IOWP are separately constrained to follow the observed SST trajectory while specifying time-evolving radiative forcing agents throughout 1920–2013. This experimental framework will likely help overcome limitations related to simplified model physics (Li *et al* 2016), such as the reduced-gravity ocean-atmosphere model (Kucharski *et al* 2011) and the slab ocean-atmosphere model (McGregor *et al* 2014), and more rigorously quantify the full extent of trans-basin interactions. The simulated magnitudes of PWC response to the eastern Pacific-induced (-1.64 ms^{-1}/35 yr and 0.74 hPa/35 yr) and North Atlantic-induced (-1.68 ms^{-1}/35 yr and 0.57 hPa/35 yr) trans-basin variabilities are both consistently underestimated by ∼40% (figure 1(c)). The underestimation is probably because the simulated trends are estimated from the ten-member average and merely represent the potential strength of PWC forced by the eastern Pacific or North Atlantic. Additionally, the notable model-observation mismatch may originate from model biases in simulating the observed large-scale SST-dipole pattern (figure 2(a)), characterized by a cold-phase IPO-SST anomaly in the Pacific-wide basin, a north-south dipole-like SST anomaly over the Atlantic, and basin-scale warming in the Indian Ocean. More importantly, tropical Pacific triangular-like cooling anomalies and Atlantic north-minus-south meridional SST gradients are qualitatively well-simulated except for the misrepresented Atlantic meridional SST gradients in the eastern Pacific-pacemaker simulations (cf figures 2(c) and (e)).

The observed PWC displays a positive trend of stream function between 120° E and 140° W (clockwise rotation) and a negative trend to the east of 140° W (anticlockwise), accompanied by descending motion in the central-eastern Pacific and ascending motion across the Maritime Continent and most of the Atlantic sector (figure 2(b)). This decadal atmospheric circulation change corresponds to a significant westward-shifted PWC (Ma and Zhou 2016, Li *et al* 2021). The North Atlantic warming initiates stronger ascending motions in the equatorial Atlantic and stronger descending motions in the equatorial central Pacific, leading to a too-far westward-displaced PWC (figure 2(f)). By comparison, the eastern Pacific cooling drives the observed westward shifting more realistically (figures 2(b) and (d)). Because of the common mean-state SST biases over the tropical Atlantic and Pacific (Kajtar *et al* 2018, McGregor *et al* 2018, Li *et al* 2020), the simulated subsidence over the central-eastern equatorial Pacific and ascent in the Maritime Continent are generally weaker than observations. Also, the observed precipitation increase illustrates a westward migration from the central Pacific to the Maritime Continent (figure 3(a)), in line with the surface wind convergence center occupying the Maritime Continent and a slight northward migration of inter-tropical convergence zone (ITCZ) across the tropical Atlantic–Pacific. The North Atlantic warming excites the decadal changes in atmospheric convection (figure 3(c)), with a too-strong northward ITCZ shift, primarily owing to the intensified Atlantic north-minus-south meridional SST gradients (Levine *et al* 2018). The eastern Pacific cooling causes a too-weak northward ITCZ displacement (figure 3(b)), albeit with surface wind convergence

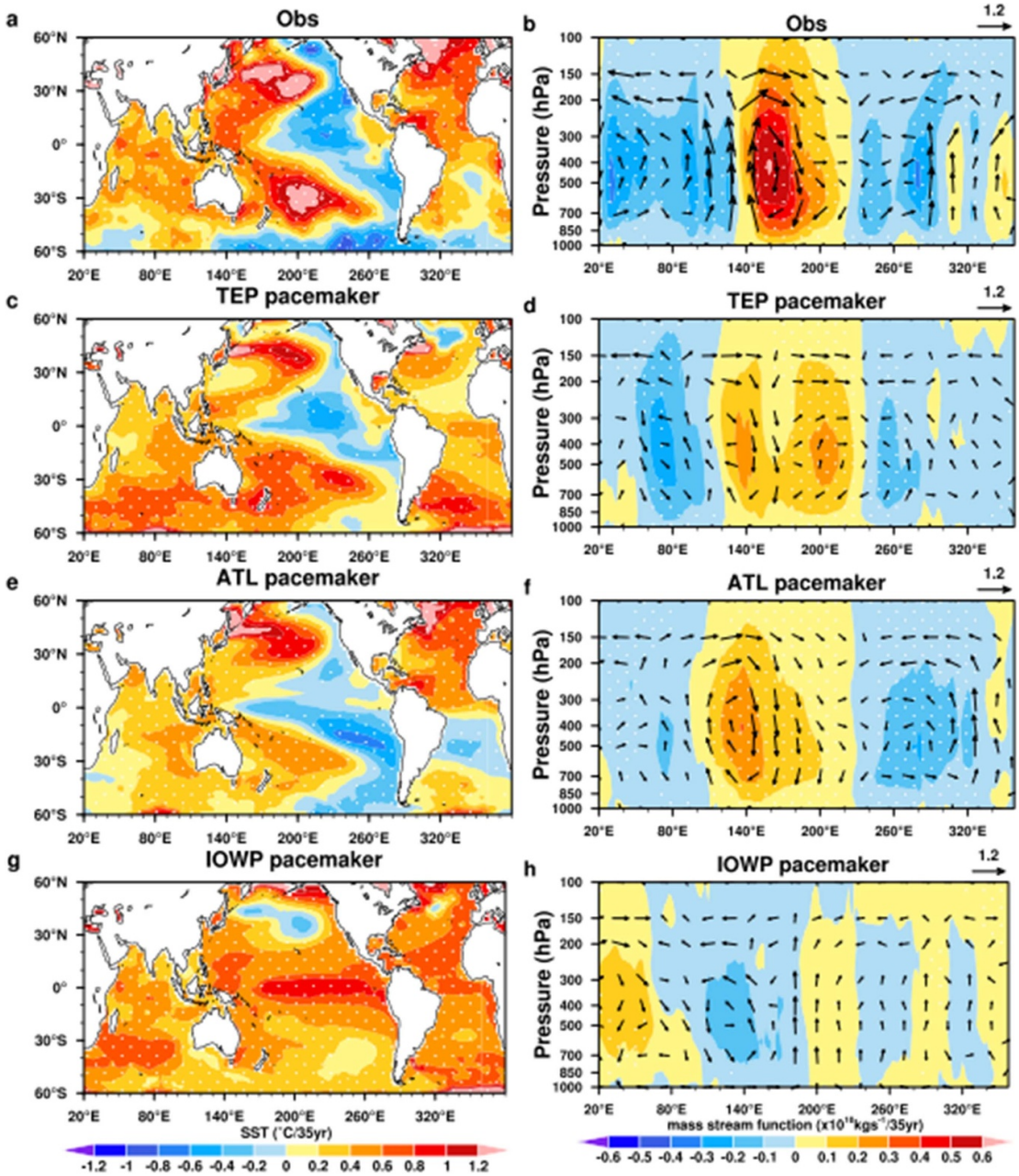

Figure 2. The observed and simulated SST (left panel) and Walker circulation (right panel) trends for 1979–2013. (a) Observed SST trends are from ERSST V3b, and (b) mass stream function trends are based on the four-reanalysis dataset ensemble average. The simulated trends are calculated from a ten-member ensemble of tropical eastern Pacific pacemaker simulations (TEP; (c)–(d)), North Atlantic Ocean pacemaker simulations (ATL; (e)–(f)), and tropical Indian Ocean-western Pacific pacemaker simulations (IOWP; (g)–(h)), respectively. The zonal mass stream function is computed by vertically integrating meridional-mean divergent wind (5° S to 5° N) from the top level downward (shading; overlying vectors representing divergent zonal wind and vertical velocity, which is magnified by a factor of 50 to make its scale comparable to the divergent zonal wind). Positive values mark a clockwise rotation, representing an enhanced Walker circulation. Stippling denotes regions with statistically significant trends above the 95% confidence level based on the Mann–Kendall test.

over the Maritime Continent. The statistical analysis also supports that the warm-phase AMV-induced easterly wind anomalies extend to the Maritime Continent (figure 3(e)), with a strong northward-shifted ITCZ over the central-eastern North Pacific. In contrast, the cold-phase IPO-induced easterly wind anomalies are only confined to about 150° E (figure 3(d)). As corroborated in the idealized IPO and AMV pacemaker experiments (figure S6), a cold-to-warm phase shift of AMV induces a too-far westward migration of PWC.

Another salient feature is the corresponding inter-basin shift of observed atmospheric pressure centers (figure S7(a)), with increasing SLP in the eastern Pacific and decreasing SLP extending from the tropical Atlantic through the Indian Ocean to the western Pacific. The large-scale inter-basin SLP see-saw responses in the North Atlantic-pacemaker and

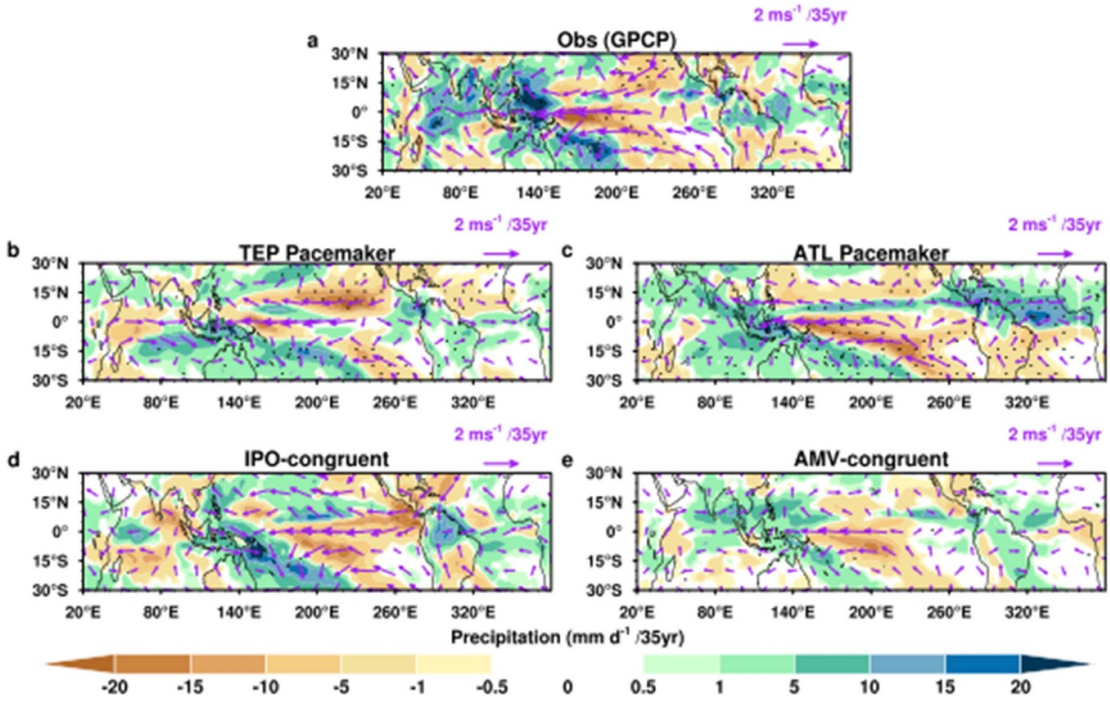

Figure 3. Observed and simulated trends of precipitation and 850 hPa winds for 1979–2013. (a) The observed precipitation trend is based on GPCP V2.3, and 850 hPa winds are estimated from 20CR V3. (b)–(c) The simulated trends are calculated from a ten-member ensemble of tropical eastern Pacific pacemaker simulations (b; TEP) and a ten-member ensemble of North Atlantic pacemaker simulations (c; ATL). (d)–(e) Observed precipitation and 850 hPa winds trends are linearly congruent with observed trends in the IPO index (d; IPO-congruent) and AMV index (e; AMV-congruent) for 1979–2013, respectively.

tropical eastern Pacific-pacemaker experiments agree well with observations (figures S7(b) and (c)), albeit at diminished magnitudes. However, the magnitudes and spatial extents of tropical eastern-central pressure lobes forced by the eastern Pacific cooling are much larger and wider than those induced by the North Atlantic warming. The support from the statistical analysis and idealized pacemaker simulations further demonstrate that a cold-phase IPO plays a larger role in triggering the trans-basin SLP see-saw pattern than a warm-phase AMV (figures S7(e)–(j)). In summary, the comparison between the observed and pacemaker-simulated results indicates that the decadal strengthening and westward shift of PWC for 1979–2013 arise mostly from combined effects of the North Atlantic warming and tropical eastern Pacific cooling, rather than SST changes in one basin alone.

We further evaluate the importance of trans-basin SST variability generated by the tropical IOWP. SST warming across the IOWP erroneously produces a reduced PWC (0.70 ms^{-1}/35 yr and −0.55 hPa/35 yr in figure 1(d)) in the absence of eastern tropical Pacific cooling and an increased north-minus-south Atlantic SST gradient (figure 2(g)). The tropical IOWP warming-induced trans-basin SST variability is insufficient to drive a significant westward-displaced PWC (figure 2(h)), contrary to previous findings that the tropical Indian Ocean rapid warming forces surface easterly wind anomalies in the whole tropical Pacific (Luo *et al* 2012, Han *et al* 2014). This discrepancy may be because a warmer western Pacific SST induces an intensified warming contrast between the tropical Pacific and Indian Oceans, accompanied by increased precipitation in the equatorial Pacific and reduced precipitation in the Maritime Continent (figure S8), in good agreement with the warmer-get-wetter view (Xie *et al* 2010). The atmospheric deep convection shift is tightly associated with surface westerly wind anomalies covering the tropical Pacific, potentially counteracting surface easterly wind anomalies occupying the tropical Pacific typical of a secondary circulation driven by a tropical Indian Ocean-only warming, as identified in a new study using the stand-alone atmosphere model forced by a steady warming rate of western Pacific SST (Han and Zheng 2023). Notably, a tropical eastern Pacific-only cooling and a North Atlantic-only warming in pacemaker simulations both excite anomalous easterly winds over the western-central tropical Pacific and anomalous westerly winds over the eastern Pacific (figures 3(b) and (c)), a surface wind divergence pattern somewhat similar to the observed (figure 3(a)). These findings support the notion that the tropical Indian Ocean tends to act as an intermediate to maintain the Atlantic–Pacific inter-basin interactions on the decadal timescales (Li *et al* 2016, Yao *et al* 2021).

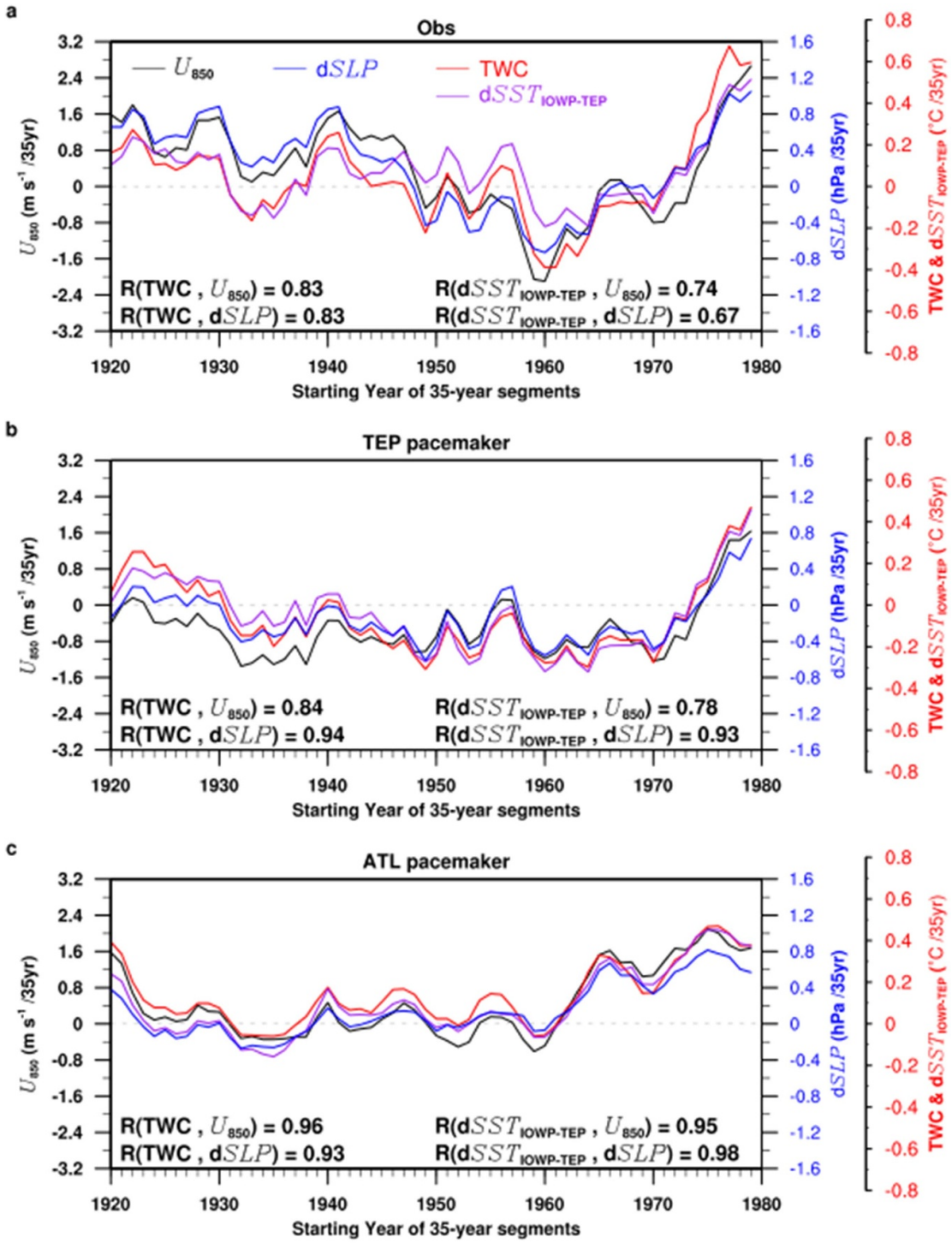

Figure 4. The observed and simulated relationship between decadal changes in the Pacific Walker circulation strength and the inter-basin SST gradients. The tropical AtlanticPacific trans-basin SST gradient (denoted TWC) is defined as the area-averaged tropical Atlantic SST (15° S–15° N, 70° W–20° W) minus the area-averaged tropical eastern Pacific SST (15° S–15° N, 180° to the American coast). The tropical Indian Ocean-Pacific inter-basin SST gradient (denoted $dSST_{IOWP-TEP}$) is defined as the area-averaged tropical Indian Ocean-western Pacific SST (15° S–15° N, 40° E–180°) minus the area-averaged tropical eastern Pacific SST (15° S–15° N, 180° to the American coast). The PWC strength is measured by the area-averaged 850 hPa zonal winds (denoted U_{850}) over the western-central Pacific (5° S–5° N, 150° E–150° W), and the area-averaged zonal SLP difference (dSLP) between the eastern Pacific (5° S–5° N, 160° W–80° W) and the eastern Indian Ocean-western Pacific (5° S–5° N, 80° E–160° E). For ease of comparison with the trans-basin SST gradients, U_{850} is multiplied by −1. Shown are temporal evolutions of sliding-window 35 year trends of U_{850} (solid black curves), dSLP (solid blue curves), TWC (solid red curves), and $dSST_{IOWP-TEP}$ (solid purple curves). (a) The observed U_{850} and *dSLP* are calculated from NOAA 20th reanalysis version 3 reanalysis, and TWC and $dSST_{IOWP-TEP}$ are estimated from the ensemble mean of seven different SST datasets. The simulated results are based on a ten-member ensemble of tropical eastern Pacific pacemaker simulations (b; TEP) and a ten-member ensemble of North Atlantic pacemaker experiments (c; ATL). The correlation coefficients between PWC strength (U_{850} and dSLP) and trans-basin SST gradients (TWC and $dSST_{IOWP-TEP}$) are shown together with the two-sided $P = 0.05$ level in each figure.

3.3. PWC decadal variations linked to tropical Atlantic-eastern Pacific SST gradients

Our model-simulation results reveal that the tropical eastern Pacific cooling and North Atlantic warming work together to drive the PWC decadal strengthening. Previous findings have shown that the Atlantic rapid warming, especially in the tropical Atlantic domain (Ruprich-Robert *et al* 2017, Yao *et al* 2021), partly amplifies recent tropical eastern Pacific cooling (Kucharski *et al* 2011, McGregor *et al* 2014, Li *et al* 2016, Ruprich-Robert *et al* 2017, Yao *et al* 2021), highlighting an active role of the Atlantic–Pacific inter-basin SST variability in modulating the PWC intensity. To illustrate the tropical Atlantic–Pacific inter-basin SST variability, we define a trans-basin warming contrast index as the difference of the area-averaged tropical Atlantic SST (15° S–15° N, 70° W–20° W) minus the area-averaged tropical eastern Pacific SST (15° S–15° N, 180° to the American coast). This definition precludes the potential impact of tropical western Pacific involving a common too-far westward-extended cold tongue in most coupled models (Luo *et al* 2018), enabling us to quantify the Atlantic–Pacific trans-basin decadal SST variability more reliably than previous approaches (McGregor *et al* 2014, 2018).

The tight relationship between the Atlantic–Pacific trans-basin warming contrast and PWC strength is well exemplified by time series of moving-window 35 year trends in tropical Atlantic–Pacific trans-basin SST gradients (TWC), 850 hPa zonal winds averaged over the western-central equatorial Pacific (denoted U_{850}), as well as the zonal SLP gradients (denoted *dSLP*) between the equatorial eastern Pacific minus equatorial eastern IOWP (figure 4). The observed decadal changes in the tropical Atlantic–Pacific trans-basin SST gradients (TWC) and PWC strength are significantly correlated (figure 4(a)), with two correlation coefficients of 0.83 ($P < 0.05$), larger than correlations between the tropical Indian Ocean/western Pacific-minus-eastern-Pacific trans-basin SST gradients and PWC strength ($r = 0.74$ and 0.67, significant $P < 0.05$), suggesting a higher dependence of observed PWC decadal variability on the tropical Atlantic-minus-eastern-Pacific inter-basin SST gradients. Similarly, the simulated tropical Atlantic-eastern Pacific trans-basin warming contrast presents a better connection with the PWC intensity in the tropical eastern Pacific- (figure 4(b)) and North Atlantic-pacemaker experiments (figure 4(c)). But this connectivity is distinct for both pacemaker simulations over the past century. From the 1920s to 1960s, the simulated coherence between the tropical Atlantic-eastern Pacific SST gradients and PWC strength is roughly close to observations (cf figures 4(a)–(c)), indicating that the tropical eastern Pacific and Atlantic SSTs are both influential in mediating the PWC decadal variability. From the 1970s onwards, an enhanced coherence between these two is only seen in the tropical eastern Pacific-pacemaker simulations and observations (figures 4(a) and (b)), emphasizing the dominant role of tropical eastern Pacific SSTs in recent decades.

4. Summary

Based on three targeted coupled model experiments where SSTs over the tropical eastern Pacific, North Atlantic, and tropical Indian-western Pacific are separately constrained to follow the observed history, along with idealized pacemaker simulations with observed IPO-SST and AMV-SST anomalies prescribed, we conduct a comprehensive analysis of underlying mechanisms of the PWC decadal variability. Our analysis suggests that a cold-phase IPO or warm-phase AMV alone cannot fully account for the observed PWC decadal strengthening for 1979–2013. During the modern satellite-monitoring era, the westward shift of observed PWC is largely driven by North Atlantic rapid warming, albeit with a simulated too-strong westward displacement. The related inter-basin shift of atmospheric surface pressure centers originates mostly from strong SST cooling in the tropical eastern Pacific. Furthermore, with strong support from observations and time-evolving pacemaker simulations, the results reveal that tropical Atlantic-eastern Pacific trans-basin SST gradients are the leading cause of the PWC decadal changes over the past century. Our findings provide an alternative explanation to the prevalent view that the Atlantic extensive warming tightly related to a warm-polarity AMV dominates the PWC decadal strengthening since the 1990s (McGregor *et al* 2014).

In addition to the dynamic tropical pathway driving the PWC decadal variability, the extratropical pathway may influence the PWC decadal changes through ocean circulation adjustments to extratropical forcing. One possible explanation is that radiative cooling of either hemisphere causes colder subsurface water upwelling in the eastern equatorial Pacific, leading to an intensified zonal SST gradient in the equatorial Pacific and hence an enhanced PWC (Kang *et al* 2020). However, the validity of extratropical aerosol-forced cooling of either hemisphere for 1979–2013 proves false because the anthropogenic-aerosol forcing is kept approximately constant during this period (Tokarska *et al* 2020). Another view involves the ocean bridge, linking subduction in the subtropical gyre domain to upwelling in the eastern equatorial cold tongue via the shallow subtropical cells (Gu and Philander 1997). Still, the extratropical-tropical oceanic links operate on longer time scales (i.e. more than 60 years), inapplicable to the observed, shorter PWC decadal variability (Fedorov *et al* 2015, Thomas and Fedorov 2017). Therefore, tropical Atlantic-eastern Pacific trans-basin SST gradients are key to understanding the PWC decadal variability. As almost all the coupled models participating in CMIP6

produce an erroneous inter-basin warming contrast between the tropical Atlantic and eastern Pacific, distinct from the observed inter-basin SST dipole-like pattern (figure 2(a)), the observed PWC pronounced acceleration for 1979–2013 is still absent in these coupled models. Our study does not shed light on what triggers the global-scale trans-basin SST variability on decadal timescales, a fundamental issue that requires further investigation.

Data availability statement

The reanalysis datasets used here are publicly available following the websites: the 20-century reanalysis product version 3 (https://psl.noaa.gov/data/gridded/index.html), ERA-interim (https://apps.ecmwf.int/datasets/data/interim-full-daily/levtype=sfc/), ERA5 (https://cds.climate.copernicus.eu/#!/search?text=ERA5&type=dataset), JRA55 (https://climatedataguide.ucar.edu/climate-data/jra-55#:~:text=JRA%2D55%20is%20the%20first,%2DVar)%20to%20this%20period). All SST datasets related to this study are downloaded from the following websites: ERSST v3b, v4, and v5 (www.ncei.noaa.gov/products/extended-reconstructed-sst), HadISST (www.metoffice.gov.uk/hadobs/hadisst/), COBE SST and SST2 (https://psl.noaa.gov/data/gridded/index.html), Hurrell SST (https://psl.noaa.gov/data/gridded/). All model outputs are available at www.earthsystemgrid.org/dataset/ucar.cgd.ccsm4.output.html.

Acknowledgments

We thank the two anonymous reviewers for their helpful comments and suggestions. This work is supported by the Chinese Postdoctoral Innovative Talent Program (119100582Q) and the National Youth Science Foundation of China (42005134). We acknowledge the CESM large ensemble community project and the climate variability and change working group for making model output available.

Conflict of interest

The authors declare no competing interests.

References

Adler R F *et al* 2003 The version-2 global precipitation climatology project (GPCP) monthly precipitation analysis (1979–present) *J. Hydrometeorol.* **4** 1147–67

Barichivich J, Gloor E, Peylin P, Brienen R J, Schöngart J, Espinoza J C and Pattnayak K C 2018 Recent intensification of Amazon flooding extremes driven by strengthened Walker circulation *Sci. Adv.* **4** eaat8785

Bjerknes J 1969 Atmospheric teleconnections from the equatorial Pacific *Mon. Weather Rev.* **97** 163–72

Boer G J *et al* 2016 The decadal climate prediction project (DCPP) contribution to CMIP6 *Geosci. Model Dev.* **9** 3751–77

Chu P-S, Chen Y R and Schroeder T A 2010 Changes in precipitation extremes in the Hawaiian islands in a warming climate *J. Clim.* **23** 4881–900

Chu P-S and Murakami H 2022 *Climate Variability and Tropical Cyclone Activity* (Cambridge: Cambridge University Press) pp 320

Chung E-S, Timmermann A, Soden B J, Ha K-J, Shi L and John V O 2019 Reconciling opposing Walker circulation trends in observations and model projections *Nat. Clim. Change* **9** 405–12

Clement A C, Seager R, Cane M A and Zebiak S E 1996 An ocean dynamical thermostat *J. Clim.* **9** 2190–6

De Boisséson E, Balmaseda M, Abdalla S, Källén E and Janssen P 2014 How robust is the recent strengthening of the tropical Pacific trade winds? *Geophys. Res. Lett.* **41** 4398–405

Dee D P *et al* 2011 The ERA-Interim reanalysis: configuration and performance of the data assimilation system *Q. J. R. Meteorol. Soc.* **137** 553–97

Delworth T L, Zeng F, Rosati A, Vecchi G A and Wittenberg A T 2015 A link between the hiatus in global warming and North American drought *J. Clim.* **28** 3834–45

Deser C, Guo R and Lehner F 2017 The relative contributions of tropical Pacific sea surface temperatures and atmospheric internal variability to the recent global warming hiatus *Geophys. Res. Lett.* **44** 7945–54

England M H, McGregor S, Spence P, Meehl G A, Timmermann A, Cai W, Gupta A S, McPhaden M J, Purich A and Santoso A 2014 Recent intensification of wind-driven circulation in the Pacific and the ongoing warming hiatus *Nat. Clim. Change* **4** 222–7

Fedorov A V, Burls N J, Lawrence K T and Peterson L C 2015 Tightly linked zonal and meridional sea surface temperature gradients over the past five million years *Nat. Geosci.* **8** 975–80

Fyfe J C *et al* 2016 Making sense of the early-2000s warming slowdown *Nat. Clim. Change* **6** 224–8

Gu D and Philander S G 1997 Interdecadal climate fluctuations that depend on exchanges between the tropics and extratropics *Science* **275** 805–7

Han W *et al* 2014 Intensification of decadal and multi-decadal sea level variability in the western tropical Pacific during recent decades *Clim. Dyn.* **43** 1357–79

Han Z-W and Zheng X-T 2023 Intermodel uncertainty in response of the Pacific Walker circulation to global warming *Clim. Dyn.* (https://doi.org/10.1007/s00382-023-06685-y)

Heede U K, Fedorov A V and Burls N J 2020 Time scales and mechanisms for the tropical Pacific response to global warming: a tug of war between the ocean thermostat and weaker walker *J. Clim.* **33** 6101–18

Held I M and Soden B J 2006 Robust responses of the hydrological cycle to global warming *J. Clim.* **19** 5686–99

Hirahara S, Ishii M and Fukuda Y 2014 Centennial-scale sea surface temperature analysis and its uncertainty *J. Clim.* **27** 57–75

Huang B, Banzon V F, Freeman E, Lawrimore J, Liu W, Peterson T C, Smith T M, Thorne P W, Woodruff S D and Zhang H-M 2015 Extended reconstructed sea surface temperature version 4 (ERSST. v4). Part I: upgrades and intercomparisons *J. Clim.* **28** 911–30

Huang B, Thorne P W, Banzon V F, Boyer T, Chepurin G, Lawrimore J H, Menne M J, Smith T M, Vose R S and Zhang H-M 2017 Extended reconstructed sea surface temperature, version 5 (ERSSTv5): upgrades, validations, and intercomparisons *J. Clim.* **30** 8179–205

Hurrell J W, Hack J J, Shea D, Caron J M and Rosinski J 2008 A new sea surface temperature and sea ice boundary dataset for the community atmosphere model *J. Clim.* **21** 5145–53

Kajtar J B, Santoso A, McGregor S, England M H and Baillie Z 2018 Model under-representation of decadal Pacific trade wind trends and its link to tropical Atlantic bias *Clim. Dyn.* **50** 1471–84

Kang S M, Xie S-P, Shin Y, Kim H, Hwang Y-T, Stuecker M F, Xiang B and Hawcroft M 2020 Walker circulation response to extratropical radiative forcing *Sci. Adv.* **6** eabd3021
Kobayashi S *et al* 2015 The JRA-55 reanalysis: general specifications and basic characteristics *J. Meteorol. Soc. Japan Ser.* II **93** 5–48
Kosaka Y and Xie S-P 2013 Recent global-warming hiatus tied to equatorial Pacific surface cooling *Nature* **501** 403–7
Kucharski F, Kang I S, Farneti R and Feudale L 2011 Tropical Pacific response to 20th century Atlantic warming *Geophys. Res. Lett.* **38**
Kucharski F, Parvin A, Rodriguez-Fonseca B, Farneti R, Martin-Rey M, Polo I, Mohino E, Losada T and Mechoso C R 2016 The teleconnection of the tropical Atlantic to Indo-Pacific sea surface temperatures on inter-annual to centennial time scales: a review of recent findings *Atmosphere* **7** 29
L'Heureux M L, Lee S and Lyon B 2013 Recent multidecadal strengthening of the Walker circulation across the tropical Pacific *Nat. Clim. Change* **3** 571–6
Lee S-K, Park W, Baringer M O, Gordon A L, Huber B and Liu Y 2015 Pacific origin of the abrupt increase in Indian Ocean heat content during the warming hiatus *Nat. Geosci.* **8** 445–9
Levine A F, Frierson D M and McPhaden M J 2018 AMO forcing of multidecadal Pacific ITCZ variability *J. Clim.* **31** 5749–64
Li C, Dommenget D and McGregor S 2020 Trans-basin Atlantic-Pacific connections further weakened by common model Pacific mean SST biases *Nat. Commun.* **11** 1–8
Li X, Wang X, Lian T, Johnson N C, Zhu J, Chang C-H, Liu H and Wang W 2021 Local and remote SST variability contribute to the westward shift of the Pacific Walker circulation during 1979–2015 *Geosci. Lett.* **8** 1–11
Li X, Xie S-P, Gille S T and Yoo C 2016 Atlantic-induced pan-tropical climate change over the past three decades *Nat. Clim. Change* **6** 275–9
Lin I I, Pun I F and Lien C C 2014 "Category-6" supertyphoon Haiyan in global warming hiatus: contribution from subsurface ocean warming *Geophys. Res. Lett.* **41** 8547–53
Luo J-J, Sasaki W and Masumoto Y 2012 Indian Ocean warming modulates Pacific climate change *Proc. Natl Acad. Sci.* **109** 18701–6
Luo J-J, Wang G and Dommenget D 2018 May common model biases reduce CMIP5's ability to simulate the recent Pacific La Niña-like cooling? *Clim. Dyn.* **50** 1335–51
Luo Y, Lu J, Liu F and Garuba O 2017 The role of ocean dynamical thermostat in delaying the El Niño–like response over the equatorial Pacific to climate warming *J. Clim.* **30** 2811–27
Ma S and Zhou T 2016 Robust strengthening and westward shift of the tropical Pacific Walker circulation during 1979–2012: a comparison of 7 sets of reanalysis data and 26 CMIP5 models *J. Clim.* **29** 3097–118
McGregor S, Stuecker M F, Kajtar J B, England M H and Collins M 2018 Model tropical Atlantic biases underpin diminished Pacific decadal variability *Nat. Clim. Change* **8** 493–8
McGregor S, Timmermann A, Stuecker M F, England M H, Merrifield M, Jin F-F and Chikamoto Y 2014 Recent Walker circulation strengthening and Pacific cooling amplified by Atlantic warming *Nat. Clim. Change* **4** 888–92
Meehl G A, Hu A, Castruccio F, England M H, Bates S C, Danabasoglu G, McGregor S, Arblaster J M, Xie S-P and Rosenbloom N 2021 Atlantic and Pacific tropics connected by mutually interactive decadal-timescale processes *Nat. Geosci.* **14** 36–42
Merrifield M A 2011 A shift in western tropical Pacific sea level trends during the 1990s *J. Clim.* **24** 4126–38
Ruprich-Robert Y, Msadek R, Castruccio F, Yeager S, Delworth T and Danabasoglu G 2017 Assessing the climate impacts of the observed Atlantic multidecadal variability using the GFDL CM2. 1 and NCAR CESM1 global coupled models *J. Clim.* **30** 2785–810
Seager R, Cane M, Henderson N, Lee D-E, Abernathey R and Zhang H 2019 Strengthening tropical Pacific zonal sea surface temperature gradient consistent with rising greenhouse gases *Nat. Clim. Change* **9** 517–22
Slivinski L C *et al* 2019 Towards a more reliable historical reanalysis: improvements for version 3 of the twentieth century reanalysis system *Q. J. R. Meteorol. Soc.* **145** 2876–908
Thomas M D and Fedorov A V 2017 The eastern subtropical Pacific origin of the equatorial cold bias in climate models: a Lagrangian perspective *J. Clim.* **30** 5885–900
Ting M, Kushnir Y, Seager R and Li C 2009 Forced and internal twentieth-century SST trends in the North Atlantic *J. Clim.* **22** 1469–81
Titchner H A and Rayner N A 2014 The Met Office Hadley centre sea ice and sea surface temperature data set, version 2: 1. sea ice concentrations *J. Geophys. Res.* **119** 2864–89
Tokarska K B, Stolpe M B, Sippel S, Fischer E M, Smith C J, Lehner F and Knutti R 2020 Past warming trend constrains future warming in CMIP6 models *Sci. Adv.* **6** eaaz9549
Vecchi G A, Soden B J, Wittenberg A T, Held I M, Leetmaa A and Harrison M J 2006 Weakening of tropical Pacific atmospheric circulation due to anthropogenic forcing *Nature* **441** 73–76
Watanabe M, Shiogama H, Tatebe H, Hayashi M, Ishii M and Kimoto M 2014 Contribution of natural decadal variability to global warming acceleration and hiatus *Nat. Clim. Change* **4** 893–7
Williams A P and Funk C 2011 A westward extension of the warm pool leads to a westward extension of the walker circulation, drying eastern Africa *Clim. Dyn.* **37** 2417–35
Xie S-P, Deser C, Vecchi G A, Ma J, Teng H and Wittenberg A T 2010 Global warming pattern formation: sea surface temperature and rainfall *J. Clim.* **23** 966–86
Yao S L, Zhou W, Jin F F and Zheng F 2021 North Atlantic as a trigger for Pacific-wide decadal climate change *Geophys. Res. Lett.* **48** e2021GL094719
Yao S-L, Chu P-S, Wu R and Zheng F 2022 Model consistency for the underlying mechanisms for the inter-decadal pacific oscillation-tropical Atlantic connection *Environ. Res. Lett.* **17** 124006
Yao S-L, Luo J-J, Huang G and Wang P 2017 Distinct global warming rates tied to multiple ocean surface temperature changes *Nat. Clim. Change* **7** 486–91
Yu B and Zwiers F W 2010 Changes in equatorial atmospheric zonal circulations in recent decades *Geophys. Res. Lett.* **37**